RATINGS OF HIGH POWER IGBT MODULES FOR PWM INVERTERS FOR TRACTION APPLICATIONS.

Frédéric Avertin, Dinesh Chamund and Bill Findlay.

Dynex Semiconductor, Lincoln, United Kingdom.

Abstract: In the design of a PWM inverter for traction applications, the selection of the semiconductor device is made from the motor current, device operating frequency, and the cooling system. Based upon these application requirements, this paper examines the parameters influencing the choice of IGBT module, both from the module design and the module reliability. Initial calculations are used to convert motor current to average and instantaneous power dissipation and therefore average and instantaneous temperatures within the IGBT module. Using accelerated reliability data for both wire bond and solder fatigue, the temperature rises within the module are used to predict the predominant failure mechanism and therefore the life of the product for the chosen motor current requirement. By modifications to the materials employed within the module, and by a redesign of the anode emitter structure of the IGBT die, it is possible to influence the temperature rise within the module and therefore improve the reliability of the product.

1. INTRODUCTION

In recent years IGBT modules have gained popularity in PWM Inverters for traction drives as they offer a simple solution to the process of power conversion and with added advantages of improved efficiency, weight and cost reduction. However in railway traction application, the equipment designer features the reliability of the equipment as the main design criteria.
In IGBT modules the well-documented failure mechanisms are the cracking of solder at the substrate to base plate interface and the lifting of wire-bonds from the silicon surface. Both of these occur by thermal cycling of the module. A typical traction duty cycle consists of accelerating, constant cruising, decelerating and stopping for a while. During this cycle the IGBT junction and substrate temperatures rise and fall due to load current fluctuation. The designer has to limit these temperature variations according to the manufacturer's recommendation in order to achieve long term reliability. In this paper we present simple design tools in form of charts which incorporate reliability data and can be used for initial selection of IGBT modules for PWM inverter-drive.

2. MODULE DESIGN FOR IMPROVED THERMAL CYCLING

Module selection for inverter applications is primarily based upon their current and voltage ratings. However, there are another two aspects to consider which will effect the power dissipation, and therefore reliability of the module in the circuit.

1. The optimisation of the silicon design to minimise losses generated by the chips.
2. The basic module construction materials influencing the thermal impedance and the resistance to temperature cycling fatigue.

2.1 Silicon Optimisation

Energy losses within the silicon die are composed of dynamic (turn on and turn off losses) and on-state losses, and it is possible to alter the balance between these parameters in order to optimise the device performance for the application. This balance has been examined using two techniques.

Figure 2.1 Tail currents assessment with helium dose for GP801DDM18.

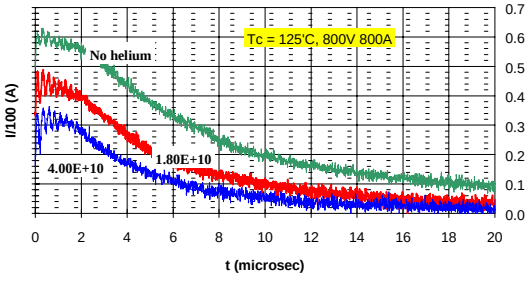

- **Helium irradiation**. Using die implanted with helium of various doses, 800A 1800V dual modules were built and their dynamic and static parameters measured. Figure 2.1 shows the effect of this implant on the turn-off tail current of the module which directly relates to the turn-off losses. As expected, increasing helium dose reduces the tail current and increases the decay rate of this tail current, leading to a reduction in turn-off losses. This however is at the expense of an increase in on- state losses, Vce(sat).
- **Anode concentration**. The second technique was to reduce the concentration of the IGBT anode. The effect on the tail current is similar, where in this case a reduction of anode concentration results in a reduced tail current and an increase in Vce(sat).

The results are best represented as an on-state, Vce(sat), vs turn-off loss, Eoff, curve where the relative merits of each technique may be assessed (see figure 2.2). Turn-on losses were hardly effected by the variation in helium dose or the change in the back implant dose. It can be seen from this trade off curve that the better process is the reduced back implant of boron rather than helium implant as they offer lower turn-off losses for the same Vce(sat).

Figure 2.2 : Vce(sat) vs Eoff

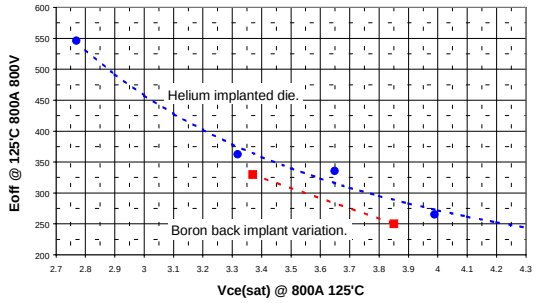

This trade-off data can be used to assess the PWM "in-circuit" performance. At higher PWM operating frequencies, lower switching losses (and therefore higher on-state losses) should offer an overall reduction in module power dissipation.

2.2 Optimum Module Construction

The module construction materials also effect the PWM "in-circuit" performance, both in terms of thermal ratings, and more importantly, in the module reliability. Two material sets were considered as part of a *standard* IGBT module construction.

- 5mm copper base plate soldered to an insulating tile of Cu/Al2O3/Cu.
- 5mm Metal Matrix Composite (MMC) base plate soldered to an insulating tile of Cu/AlN/Cu.

2.2.1 Thermal Impedance

The thermal ratings of the two material sets are represented by their transient thermal impedance curves. Figure 2.3 compares the transient thermal resistance curves for a 3D finite element and SPICE simulations of smaller IGBT die. The results show a maximum error between the two models of approximately 8% and therefore the SPICE simulation deck will be used for further work in this analysis.

Figure 2.3 : Transient Thermal resistance per die for "finite element" vs SPICE models.

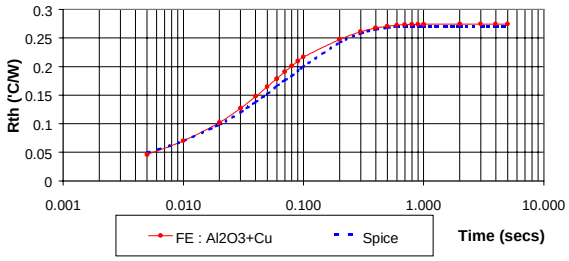

Figure 2.4 : Transient thermal impedence for 800A modules, Cu/Al2O32 and MMC/AIN.

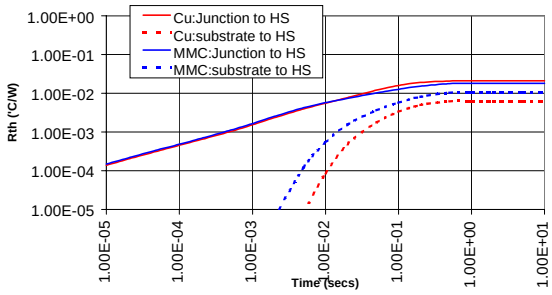

Figure 2.4 shows thermal resistance values, junction to base plate, and substrate (DCB) solder to base plate for the Cu+Al2O3 and

MMC+AlN structures. The MMC+AlN combination offers an improvement of approx. 10% in the DC thermal resistance (Rth), and a small change in Rth values for pulses around 100msec due the lower thermal resistance of the AlN.
This data is used in conjunction with the PWM inverter model to assess junction temperatures within the module for different operating conditions.

2.2.2 Thermal Cycling Fatigue

However it is the difference in reliability between these module types that forms the major basis for operating performance in the inverter circuit. Figure 2.5 summarises Dynex data and published data [2] for solder fatigue and wire bond cycles to failure. The improved matching of thermal expansion of MMC to AlN is reflected in a more that 5 fold increase in solder fatigue capability. Wire bond capability is improved by approximately 7 times by the addition of a protective coating, where the coating prevents bond lifting leading to increased Vce(sat) and ultimately chip failure.

Figure 2.5 : Wire Bond cyling and Solder fatigue.

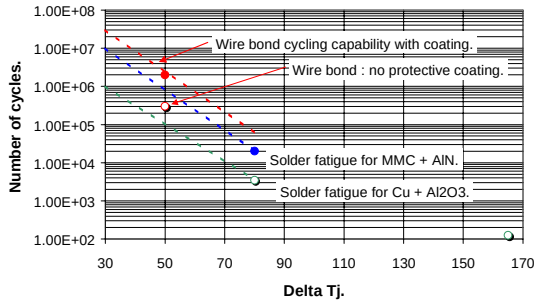

3. THERMAL ANALYSIS OF THE MODULE

Two low cost, and widely used software tools have been used to estimate the average and instantaneous elevations of temperature when the IGBT module is running in a 3 phase voltage source inverter with a sinusoidal PWM operation.

- Excel has been used to calculate the average elevation of base plate solder temperature.
- MathCad 6 has been used to provide the instantaneous junction temperature.

3.1. Base plate solder thermal stress

The base plate to substrate interface is far removed from the PWM switching events in the silicon and therefore the thermal response at this interface may be estimated using an average total power dissipation of the overall system. The DC thermal resistance can be used in these calculations.
Listed below are the basic equations used as described by D.Srajber and W.Lukash [1].
These may be used to estimate the average power losses and rise in temperature **within an arm of the inverter**.

$$Pcond_{IGBT} = \frac{1}{2}.\left(v_{0IGBT}.\frac{I_{Max}}{\pi} + r_{0IGBT}.\frac{I^2{}_{Max}}{4}\right) + m.\cos\varphi.\left(v_{0IGBT}.\frac{I_{Max}}{8} + \frac{r_{0IGBT}.I^2{}_{Max}}{3\pi}\right)$$

$$Pcond_{Diode} = \frac{1}{2}.\left(v_{0Diode}.\frac{I_{Max}}{\pi} + r_{0Diode}.\frac{I^2{}_{Max}}{4}\right) - m.\cos\varphi.\left(v_{0Diode}.\frac{I_{Max}}{8} + \frac{r_{0Diode}.I^2{}_{Max}}{3\pi}\right)$$

$$Psw_{IGBT} = \frac{1+\cos\varphi}{2\pi}.f_{sw}.E_{sw\,IGBT}$$

$$Psw_{Diode} = \frac{1+\cos\varphi}{2\pi}.f_{sw}.E_{sw\,Diode}$$

With $E_{sw_{IGBT}} = \left(E_{on} + E_{off}\right).\frac{I_{Max}}{I_{Nom}}.\frac{U_{DC}}{U_{Nom}}$ and

$$E_{sw_{Diode}} = E_{\mathrm{Re}c}.\frac{I_{Max}}{I_{Nom}}.\frac{U_{DC}}{U_{Nom}},$$

The mean power losses and the maximum temperature excursion of the base plate solder can be estimated from:

$$P\_Tot_{Module} = 2.\left(Pcond_{IGBT+Diode} + Psw_{IGBT+Diode}\right)$$

$$\Delta T_{BP-Amb} = P\_Tot_{Module}.\left(Rth\_IGBT_{\substack{BP\\-HS}} + 3.Rth\_IGBT_{HS-Amb}\right)$$

$$\Delta T_{DCB-BP} = \Delta T_{BP-Amb} + \left(Pcond_{IGBT} + Psw_{IGBT}\right).Rth\_IGBT_{DCB-BP}$$

3.2. Junction thermal stress (MathCad)

High torque is required during start up of the inverter motor and this leads to maximum current in the module. Furthermore, during this critical phase, the output frequency of the inverter is low (slip frequency of 3 to 5 Hz). Therefore, phase current values in excess of

the module maximum rating of 800A, and motor frequencies in the 3 to 10Hz were chosen for these simulations.
Outlined below are the five basic steps employed in the MathCad calculation of instantaneous junction temperature within the IGBT module. The simulation allows no feedback of chip temperatures into the module power losses, and therefore worst case values have been chosen for all the input parameters, i.e. Vo, Ro, Eon and Eoff, have been chosen at the maximum junction temperature of 125'C.

1. Input of parameters.
   → *Inverter*
   (DC link voltage, I_{rms} , F_{out} , F_{sw} , m, PF)
   → *IGBT*
   V_o , R_o , E_{on} , E_{off}, all at @ 125°C, and Zth(t),IGBT junction to base plate.
   where $Z_{th}(t) = \sum_{i=1}^{5} R_i \cdot \left[1 - \exp\left(-\frac{t}{\tau_i}\right)\right]$

2. Generation of the PWM currents in each of the switches.

3. Convert the measured IGBT dynamic parameters (Eon and Eoff) into gaussian power distributions $P_{SW}(t)$.

4. Generation of instantaneous dissipated power equations
   → $P_{cond}(t)$, $P_{sw}(t)$, $P_{Tot} = P_{cond}(t) + P_{sw}(t)$

5. Calculation of $\Delta T_{j\text{-}c}(t)$, junction temperature to base plate.

$$\Delta T_{J-C}(t) = \int_0^t P_{Tot}(\tau) \cdot dZ_{th\,J-C}(t-\tau)\,d\tau$$

where $dZ_{th\,J-C}(t) = \frac{dZ_{th\,J-C}(t)}{dt}$

An example of the output from this calculation is shown in figure 3.1 for a GP801DDM18 module. (See Section 4 for details). Power/100 and junction temperature are plotted against time for an IGBT switching frequency of 2kHz and a motor frequency of 5Hz, (which can clearly be deduced by the periodic rise and fall of junction temperature). Junction temperature ripples by approx. 32'C, where the peak value is reached just after the peak in power losses. Although the peak temperature of the junction continues to rise, the ripple for the 3 periods displayed is almost constant.

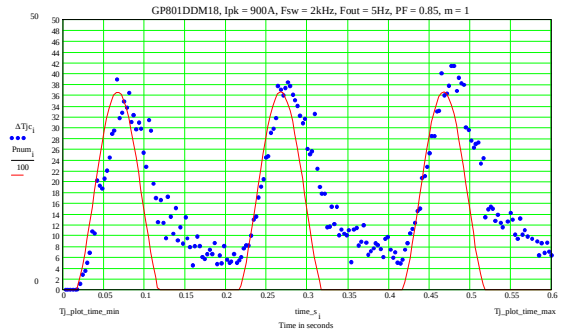

Using this MathCad deck, it is possible to estimate the periodic rise and fall of temperatures within the module for a vast range of inverter conditions, and use these temperature fluctuations to estimate the life of the module.

4. DISCUSSION.

Using the above data, PWM inverter calculations were performed for the three module types listed below and these calculations were used to estimate module life in service.

Parameter (800A 125'C)	Module A	Module B	Module C
Vce (V)	4.3	3.3	3.3
Eoff (mJ)	240	370	370
Eon (mJ)	320	320	320
Erec (mJ)	110	110	110
Rth ('C/kW)	21	21	18
Construction	Cu + Al2O3	Cu + Al2O3	MMC + AlN

Where module A: GP80**0**DD**S**18
B: GP80**1**DD**S**18
C: GP80**1**DD**M**18.

For the evaluations of base plate solder thermal stress, a DC line voltage of 900V, power factor 0.85, and modulation index of 1 was chosen. Typical values were chosen for the thermal resistance, case to heat sink, and heat sink to ambient. A summary table of these values and the module values are given in the following table.

	Module A	Module B	Module C
Rth (‘C/W) BP-HS	0.008	0.008	0.008
Rth (‘C/W) HS-Ambient	0.009	0.009	0.009
Rth (‘C/W) DCB-BP.	0.006	0.006	0.011

In this analysis, it is proposed that the selection of a module for reliability in a PWM inverter circuit may be characterised by 2 graphs:

- Slow cycling capability. This relates to the station to station situation in traction. This may be calculated using the information in section 3.1.
- Fast cycling capability. This relates to the PWM effect on the junction temperature. This is calculated from the MathCad simulation in section 3.2.

Both these cycling capabilities are represented as number of cycles vs. peak phase current of a 3-phase PWM inverter.

In order to use these curves, it is assumed that the designer has the phase current and motor frequency as a function of time, and has selected the PWM switching frequency.

4.1 Slow cycling capability.

Figure 4.1 and figure 4.2 show the slow cycling capability for module types B, (GP801DDS18), and C, (GP801DDM18), as a function of and peak phase current, at typical PWM switching frequencies of 500Hz, 1kHz, and 2kHz. The curves represent the average temperature conditions within the module, both at the junction, and at the solder interface, and cover wire bond, and solder failures resulting from these average temperatures.

Cut points are shown on the curves. These points relate to a transition between a solder failure mechanism limitation, or the wire bond limitation. However, the majority of these cut points occur at high phase currents, in excess of 800A, where the junction temperature has exceeded the maximum rating of 125’C, and it can therefore be assumed that the only relevant mechanism is the cycling of the solder at the base plate.

Since the dominant mechanism is solder fatigue, Figures 4.1 (module B) and 4.2 (module C) cover aspects of module design relating to the substrate solder. The chip set is the same.

Figure 4.1 : IGBT Thermal Cycling Capabilities for 3 Phase PWM Inverter (Module B)

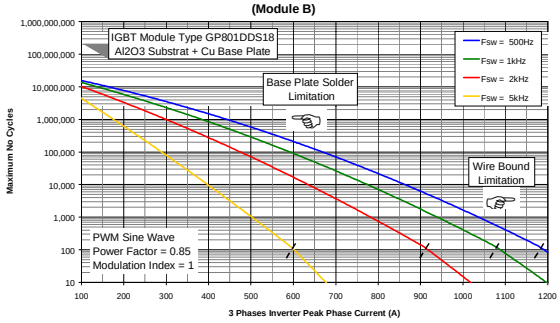

Fig 4.2 : IGBT Thermal Cycling Capabilities for 3 Phase PWM Inverter (Module C)

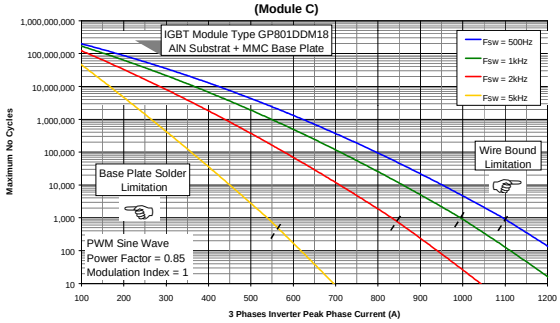

The effect of the PWM frequency on the base plate solder becomes more dominant at high phase currents and so in general the curves diverge. The materials used in the construction of module type C offer an improvement in the thermal expansion match between the base plate and the substrate, and it is this improved thermal match (and not the improved Rth) that is reflected in the 5 fold improvement in performance.

As expected, high PWM frequencies are more severe. Therefore for the fast cycling capability, modules A, B and C were compared at a typical upper operating switching frequency of 2kHz.

4.2 Fast cycling capability.

Figures 4.3, 4.4, and 4.5 show the fast cycling capability for module types A, B and C at the worst case switching frequency of 2kHz. Number of cycles to failure are plotted against phase current as before, along with inverter output frequencies 3, 5 and 10Hz. These output frequencies correspond to a typical start up situation for the inverter.

At low phase currents, performance for all 3 modules are similar and not very dependent upon the output frequency of the inverter. The low phase current produces only a small difference in ripple of the junction temperature between the module types.
However the situation is different as the phase current is increased.

Figure 4.3 : IGBT Thermal Cycling Capability of Wire Bounding for 3 Phases PWM Inverter (Module A).

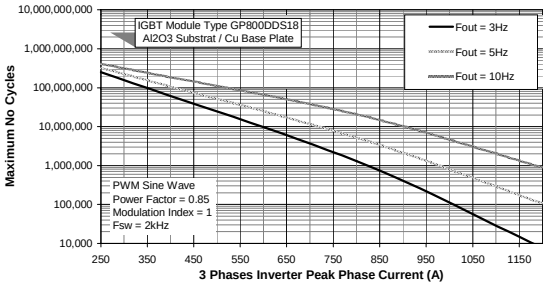

Figure 4.4 : IGBT Thermal Cycling Capability of Wire Bonding for 3 Phases PWM Inverter (Module B).

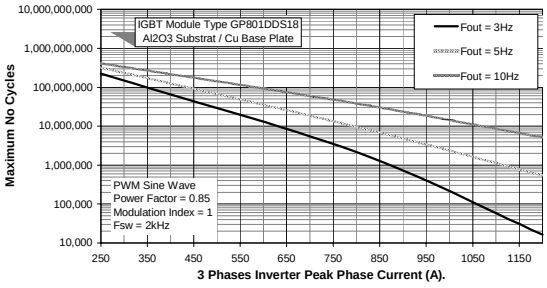

Figure 4.5 : IGBT Thermal Cycling Capability of Wire Bonding for 3 Phases PWM Inverter (Module C).

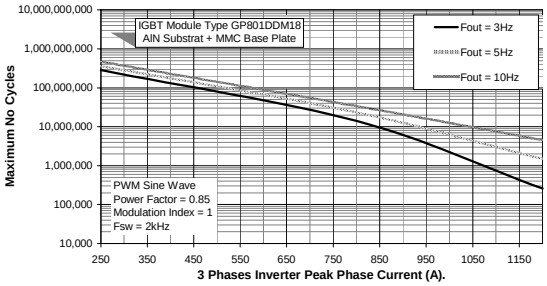

If we first consider the comparison for the chip technologies, module types A and B. Module B offers an improved performance, but the difference in performance is only significant at phase currents above 550A. Below this current the difference is around 10%. At much higher phase currents of 950A, the difference in performance improves significantly where module B offers a 2 fold increase in the cycling.
The trend is similar, but more marked comparing module technologies (modules B and C). For the minimum output frequency of 3Hz, a minor difference in performance of approx. 10% at 250A is increased to approx. 3 fold at 550A and 10 fold at 950A. This improvement decreases as the output frequency of the inverter is increased, so that at 10Hz, there is little to choose between the 2 modules.

5. CONCLUSION.

The techniques described above have proved useful in determining the parameters which influence the reliability of the module in a PWM application, both from a chip optimisation, and the module construction aspects.
These techniques have been used to quantify the reliability of a module in a PWM inverter circuit using 2 graphs, which relate to the slow cycling of the application, and the fast cycling due to the PWM current in the module.
It has shown that the most stressful situation for the PWM action is on the wire bond and is at motor start up, where phase current far exceed running current, and the inverter output frequency is low.
For the slow cycling generally associated with station to station running, the solder failure mechanism is dominant and as a result the benefit of the MMC+AlN structure over the Cu+Al2O3 is clearly evident.

References.

[1] D.Srajber and W.Lukash.
"The calculation of the power dissipation for the IGBT and the inverse diode in circuits with the sinusoidal output voltage"
Electronica 92 Proceedings, p.51-58.

[2] Schutse, Berg & Hierholzer.
"Further Improvements in the Reliability of IGBT Modules".
1998 IEEE 33rd IAS Annual Meeting.